DOI 10.5162/sensoren2024/C1.4

Different Ways to Simplify a Simulation Model of an Additively Manufactured Force Sensor with Embedded Constantan Wires as Sensing Elements in the Field of Robot Gripping Technology

Nikolai Hangst[1], *Lukas Stiglmeier* [1], *Philipp Gawron* [1], *Thomas M. Wendt* [1] *and Stefan J. Rupitsch* [2]
[1] Offenburg University of Applied Sciences, Work-Life Robotics Institute, Offenburg, Germany
[2] University of Freiburg, Department of Microsystems Engineering, Laboratory for Electrical Instrumentation and Embedded Systems, Freiburg, Germany
nikolai.hangst@hs-offenburg.de

Summary: In this contribution, we present different ways to simplify a simulation model of an additively manufactured force sensor in the field of robot gripping technology for efficient determination of results using COMSOL Multiphysics. The results of different computational approaches are compared with the required computing time and memory requirements. A simplified analytical approach is also presented as an alternative and to verify the plausibility of the simulations.

Keywords: robotic, gripping technology, sensitive gripper jaws, force sensor, simulation, additive manufacturing

Introduction

Additive manufacturing, also known as 3D printing, has evolved continuously since the first patent was granted by Chuck Hall in 1986 [1]. In particular, the trend toward complex and functional components, up to complete mechatronic systems, represents a substantial technological advance. [2–4] This trend has also established itself in robotics. For example, plastic-based individual gripper jaws with integrated sensors and adapted gripping surfaces can be realized in a single process for handling sensitive and fragile components. [5, 6] Due to these individualizations, minimizing the effort and time required to design gripper jaws for different conditions is necessary. Memory requirements must also be considered, as a simulation model can take up several GB of memory.

Preliminary Work

The basic model of the sensor consists of an arbitrary number of bending beams arranged one above the other, based on a load cell. Using this multiple-bending beam structure, it is possible to individually increase a plastic jaw's foundational stability or stiffness and simultaneously ensure deformation parallel to the initial state during a gripping process. Fig. 1 shows the basic structure of the robot gripper utilizing the example of gripping a chicken egg, consisting of two gripper jaws with seven bending beams each. In addition to improving the stability of the sensor, the embedding of constantan wires as sensing elements in each bending beam of the gripper jaw elevates the sensor's linearity and viscoelastic behavior. The PETG plastic carrier and the sensor elements forms a composite material and thus serves as a reinforcement. Each bending beam has two sensor elements at the top and bottom to absorb compressive and tensile stresses.

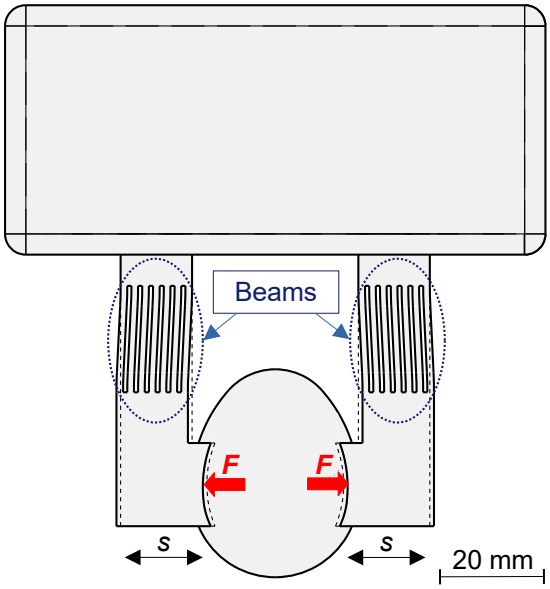

Fig. 1: Basic structure of the robot gripper with seven bending beams per gripper jaw.

Simplified Sensor Design

The sensor design was reduced to an output model with a minimum number of two bending beams to compare different calculation approaches. Another feature was the omission of the gripping surface, which is considered irrelevant for the simulation as it does not affect the results. Fig. 2 shows the new sensor variant with the force application F and the resulting stresses $\sigma_{tens_{1,2}}$ and $\sigma_{comp_{1,2}}$ in the embedded sensor el-

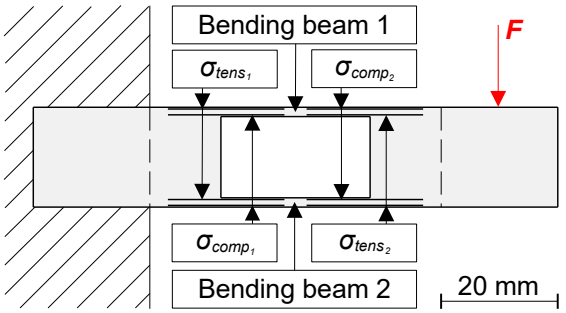

Fig. 2: Simplified sensor model with two bending beams and eight sensor elements.

ements. The sensor's dimensions are 90 mm x 17.2 mm x 20 mm (length, height, depth) with a respective beam thickness of 1.6 mm each. Each bending beam contains four meandering resistive sensor elements made of constantan wire with a total measurement grid length of 20 mm and a distance of 0.3 mm to the respective surface. A sensor element consists of 22 adjacent resistive wire paths in the grid without connecting wires. The wire length for one of the sensor elements σ_{tens_1} or σ_{comp_1} on the left is 526 mm, and for one of the sensor elements σ_{tens_2} or σ_{comp_2} on the right is 620 mm. The difference is due to the connection wires on the left side of the sensor. Under load, two sensor elements are subjected to tension and two to compression. The evaluation is carried out using a Wheatstone half-bridge.

Materials and Methods

Polyethylene terephthalate glycol (Prusament PETG Signal White, Prusa Research) was used as the non-conductive material for the calculations. The conductive material was constantan wire (CuNi44, DM 0.2 mm, VDM-Metals). The mechanical and electrical properties of the materials were taken from the material data sheets and are shown in Tab. 1. The k-factor was taken from the value of a classical strain gauge. The finite element analysis of each simulation model was performed using COMSOL Multiphysics. The computer system applied was an Intel® Core™ i7-10750H CPU with 32 GB of RAM. The analytical approach was performed utilizing MATLAB.

Analytical Approach

An analytical approach with the following simplified assumptions can approximate the behavior of the sensor:

- Two-dimensional view.
- Ideal parallel deformation of the sensor using a fixed end on one side and a vertical parallel movement on the opposite side.

Tab. 1: Mechanical and electrical properties of the applied materials [7].

Parameter	PETG	Constantan
Yield-strength	47 MPa	250 MPa
Young's-modulus	1500 MPa	165000 MPa
Poisson's-ratio	0.40	0.33
Density	1270 kg·m^{-3}	8900 kg·m^{-3}
Conductivity	-	4.9·10^{-7} Ω·m
k-factor	-	2.05

- Considering only one of the 1,6 mm thick bending beams for the mechanical calculation. The transition to the standard beam and the leads are ignored (the measurement length of a sensor element is less than the total measurement grid length of a sensor element).
- Ignoring Poisson's ratio in the mechanical part.
- Formation of an idealized fiber composite material with a homogeneous Young's modulus for the individual sensor elements.

The calculation of the sensor behavior is divided into a mechanical and an electrical part. First, the effective length change $|\Delta l_{ges}|$ across all sensing elements is calculated. Then, the differential voltage U_D can be determined. Fig. 3 shows the simplified sensor's model of a bending beam from Fig. 2, including the parallel deformation represented by the bending line $w(x)$. For reasons of symmetry and the resulting relationship between eq. (1) and eq. (2):

$$l_{M_{12}} = l_{M_{34}} = l_{M_{56}} = l_{M_{78}} \tag{1}$$

$$\Delta l_{M_{12}} = -\Delta l_{M_{34}} = -\Delta l_{M_{56}} = \Delta l_{M_{78}} \tag{2}$$

it is sufficient to consider one sensor element of the bending beam (in our case, Fig. 3, top left) for the calculation. The bending moment $M(x)$ must first be determined to calculate the strain ε_{12} and thus the change in length $\Delta l_{M_{12}}$. Due to the body's static indeterminacy, it is impossible to ascertain this function from the support reactions. According to Euler-Bernoulli, the 4th order differential equation of the bending line w from the beam theory as given in eq. (3) is used as the basis.

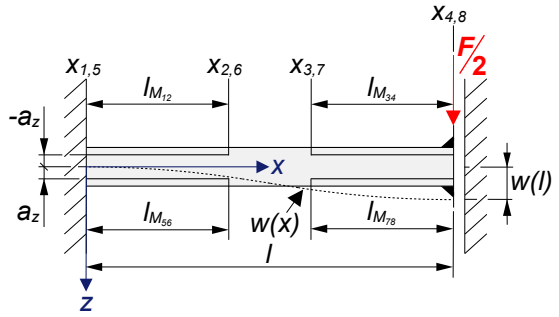

Fig. 3: Sketch of the simplified sensor model with one of the two bending beams.

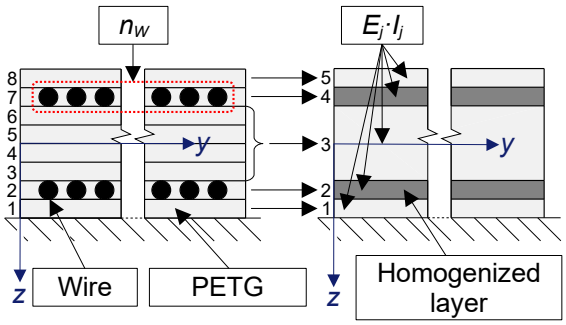

Fig. 4: Schematic sectional view of the bending beam, (left) printed layers with integrated constantan wire, (right) formation of combined homogeneous layers.

$$\sum_{j=1}^{s} E_j I_j w^{IV} = q_0 \tag{3}$$

The sum of E_j and I_j corresponds to the bending stiffness of the composite material, and q_0 is the acting line load or the dead weight of the beam. Due to $F/2 \gg q_o$, this value can be simplified to zero. A multilevel integration of eq. (3) and the use of appropriate boundary conditions results in

$$M(x) = \frac{F}{2}\left(x - \frac{l}{2}\right). \tag{4}$$

This equation can determine the strain ε_{12} of the sensor element σ_{tens_1} regarding its measuring grid length $l_{M_{12}}$ according to

$$\varepsilon_{12} = \frac{\frac{1}{x_2 - x_1}\int_{x_1}^{x_2} M(x)\,dx}{\sum_{j=1}^{s} E_j I_j} \cdot (-a_z). \tag{5}$$

The individual Young's moduli E_j consists of the PETG matrix and the composite material with an additional proportion of constantan. An idealized composite based on a homogeneous Young's modulus is used for the embedded wire layers for analytical consideration. Fig. 4 shows a schematic sectional view of the bending beam through two sensor elements, including the formation of homogeneous layer areas. The effective Young's modulus of the homogeneous layers 2 and 4 is to be determined proportionally from the respective Young's modulus E_j of PETG and constantan and its volume fraction using

$$E_{eff} = E_W \cdot V_W + E_P(1 - V_W). \tag{6}$$

E_W and E_P are Young's modulus of constantan and PETG, respectively, and V_W is the corresponding volume fraction of the wire. The second moment of area I_j is obtained from eq. (7) based on the parallel axis theorem.

$$I_j = I_{Y_j} + z_{s_j}^2 A_j \tag{7}$$

I_{y_j} is the second moment of the areas, z_{s_j} is the distances of the single area centroids from the total centroid, and A_j is the areas of the different homogeneous layers from Fig. 4 on the right. After calculating the strain ε_{12}, the effective change in length of the wire must be determined considering all the sensor elements according to

$$|\Delta l_{ges}| = 8 \cdot l_{M_{12}} \cdot n_w \cdot \varepsilon_{12}. \tag{8}$$

The number 8 represented the total number of sensor elements of the sensor, $l_{m_{12}}$ is the measuring length of one sensor element, and n_W is the number of wire paths per sensor element. After determining the mechanical characteristics, the differential voltage U_D is calculated using a Wheatstone half-bridge, expressed by

$$U_D = \frac{1}{2} U_0\, k \left(\frac{|\Delta l_{ges}|}{l_{ges}}\right). \tag{9}$$

U_0 is the output voltage, k is the k-factor, and l_{ges} is the total wire length of all sensor elements, including the connecting leads.

Sensor Simulation

The simulation is founded on the initial model shown in Fig. 2 with the two bending beams. It is based on a linear-elastic model with homogeneous and isotropic material properties for PETG and constantan (listed in Tab. 1) and a stationary study. The different approaches range from a unidirectional coupled analysis to a simplified simulation with homogeneous plates (see Fig. 5). The first and most complex calculation approach for sensitive gripper jaws is

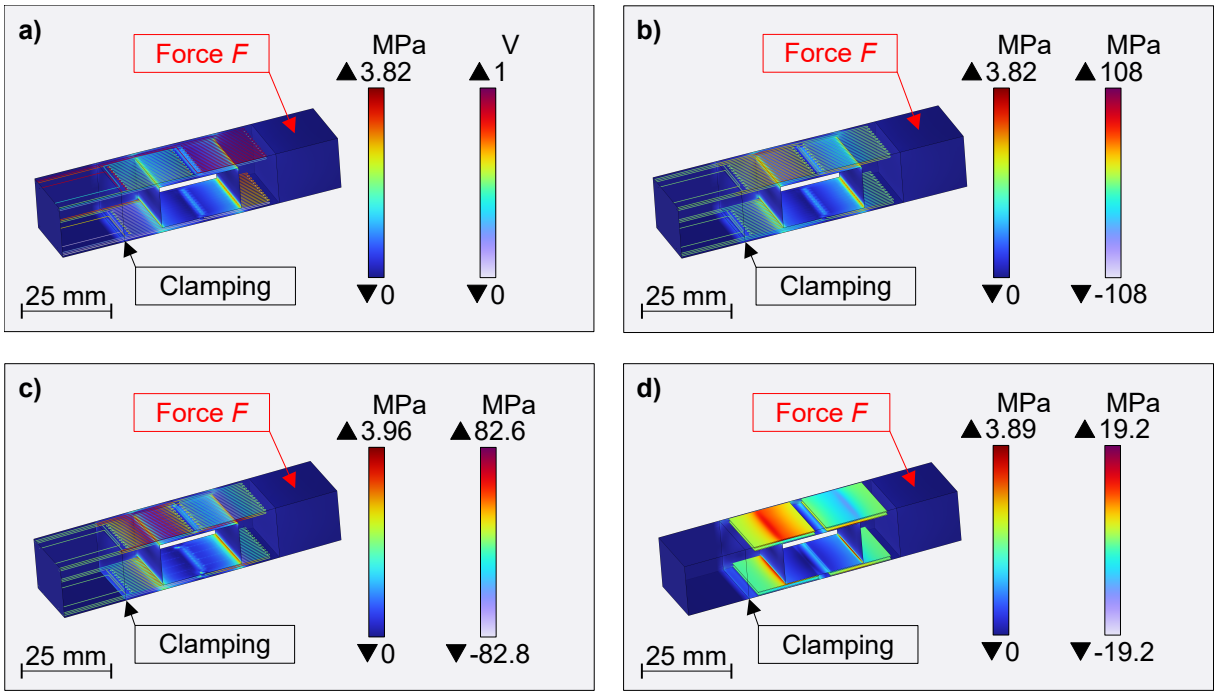

Fig. 5: Representation of the Mises equivalent stresses in the beam and the electrical Voltage or normal stresses in the sensor elements of the different calculation approaches at a force F of 10 N. a) unidirectionally coupled simulation with solid elements (reference approach), b) combination of simulation with solid elements and analysis (alternative calculation approach 1), c) combination of simulation with solid and beam elements and analysis (alternative calculation approach 2), d) combination of simulation with homogeneous plates and analysis (alternative calculation approach 3).

the reference approach with a unidirectional coupling between the mechanical and electrical part (see Fig. 5a). Here, a differential voltage is calculated on a Wheatstone half-bridge circuit from an applied force F via the resulting deformation of the spring body and the resulting changes in length of the sensing elements. The force F was employed in five steps: 0 N, 2.5 N, 5 N, 7.5 N, and 10 N. The maximum force F of 10 N is obtained by considering the constantan's yield strength, including a safety factor greater than 2. The safety factor can be determined by Hangst et al. [7].

A first simplification of the calculation is to perform a purely mechanical simulation followed by an analytical calculation according eq. (9) of the differential voltage at the measuring bridge (see Fig. 5b). A further simplification option is to consider the constantan wire as a fiber reinforcement. The wire is not considered a three-dimensional volume element in the mechanical analysis. Nevertheless, as a fully coupled one-dimensional beam element (see Fig. 5c), the number of degrees of freedom is reduced, positively affecting the computation time. The last approach can be traced back to a simplified model in which the individual wires of a sensor element are each combined and calculated to form a homogeneous pad with an effective Young's modulus (see eq. (6)) consisting of wire and PETG material (see Fig. 5d). This calculation approach is similar to the analytical approach but without the simplifications in the bullet points.

Results and Discussion

The results of the sensor behavior of all calculation approaches, including the analytical approach, are shown in Fig. 6. The alternative calculation approaches 1 and 2 show similar results compared to the reference approach. The maximum deviation of 0.6 % is due to differences in the mesh and calculation approaches. The simplified calculation approach with the homogeneous plates as sensor elements (alternative calculation approach 3) deviates more strongly from the reference at -2.9 %. This is due to the stiffer behavior of the homogeneous plate compared to the individual wires. In addition, the connecting leads were neglected for further simplification. The most substantial deviation from the reference is due to the analytical approach. The deviation of -27.1 % results from the large number of simplified assumptions. Nevertheless, the analytical approach provides a good approximation of the sensor behavior and can, therefore, be used to check the plausibility of the simulations.

The relative differences in computation time and memory requirements of the calculation approaches compared to the reference are shown

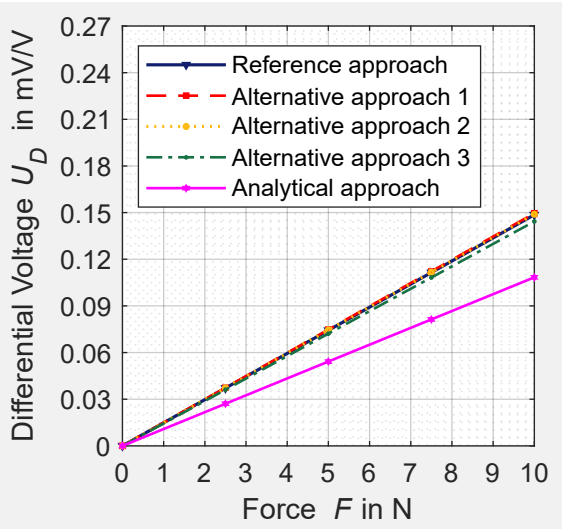

Fig. 6: Sensor behavior of the different calculation approaches.

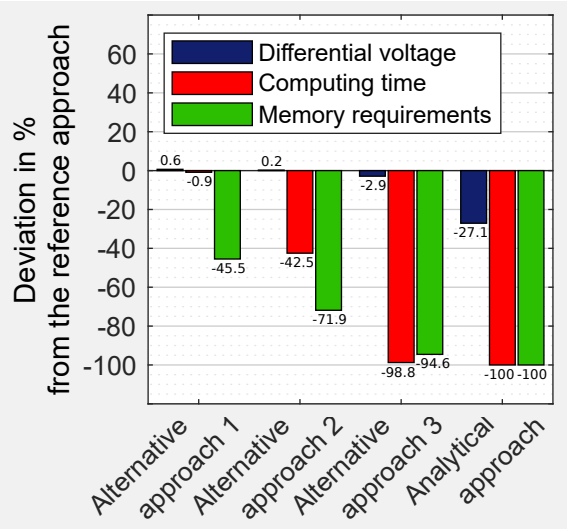

Fig. 7: Relative differences in terms of differential voltage, mesh quality, computation time, and memory requirements of the different calculation approaches compared to the reference model.

in Fig. 7. For better comparability, the relative differences of the differential voltages U_D are also shown. The computation time decreases continuously with the alternative calculation approaches due to simplifying the meshes based on reduced degrees of freedom. This also reduces the memory requirements. The analytical approach does not require a mesh, so the computational time and memory requirements are negligible. The absolute values for computation time and memory requirements for all calculation approaches are shown in Tab. 2. For completeness, the values for the sensor behavior at F = 10 N, and the number of degrees of freedom is shown. The number of degrees of freedom is an expression of the complexity of the mesh. With more degrees of freedom, the mesh becomes more complex.

Regarding the complexity of the simulation model, the alternative calculation approach 2 is the most suitable. On the one hand, the differences of 0.2 % between the results and the reference are minimal, but the computation time of -42.5 % and memory requirements of -71.9 % are significantly more efficient. Secondly, the wire does not have to be modeled as a three-dimensional volume model but only as a one-dimensional wire model. This means that both components are initially independent and are only combined in the calculation itself via a bidirectional coupling.

Conclusion and Outlook

In this contribution, it has been shown that by using different calculation approaches, corresponding savings in computational time and memory can be achieved with minor deviations in the results. A simplified analytical approach without finite element analysis also provides first insights into the sensor behavior. This approach can also be used to check the plausibility of the simulation results.

In the future, the extent to which the two-beam sensor model can be transferred to a sensor model with a variable number of bending beams without a new simulation will be investigated. This would have the advantage of saving additional computation time and memory.

References

[1] R. Lachmayer, R. b. Lippert, and T. Fahlbusch, 3D-Druck beleuchtet. Berlin, Heidelberg: Springer Berlin Heidelberg, 2016.

[2] D. Espalin, D. W. Muse, E. MacDonald, and R. B Wicker, ”3D Printing multifunctionality: Structures with electronics,” Int J Adv Manuf Technol, vol. 72, 5-8, pp. 963–978, 2014, doi: 10.1007/s00170-014-5717-7.

[3] Y. Song, R. A. Boekraad, L. Roussos, A. Kooijman, C. C. L. Wang, and J. M. P. Geraedts, “3D Printed Electronics: Opportunities And Challenges From Case Studies,” in Volume 1: 37th Computers and Information in Engineering Conference, Cleveland, Ohio, USA, 2017.

[4] K.-Y. Joung, S.-Y. Kim, I. Kang, and S.-H. Cho, “3D Printed Load Cell Using Nanocarbon Composite Strain Sensor,” Sensors (Basel, Switzerland), vol. 21, no. 11, 2021, doi:10.3390/s21113675.

[5] M. N. Saadatzi, S. K. Das, I. B. Wijayasinghe, D. O. Popa, and J. R. Baptist, ”Precision Grasp Control with a Pneumatic Gripper and a Novel Fingertip Force Sensor,” in 2018 IEEE 14th International Conference on Automation Science and Engineering (CASE), Munich, Germany, 82018, pp. 1454–1459.

Tab. 2: Results of the different calculation approaches.

Label	U_D ($F = 10\,\mathrm{N}$)	Degrees of freedom	Computing time	Memory requirements
Reference approach	0.14862 mV/V	5,043,950	34.67 min	932 MB
Alternative approach 1	0.14956 mV/V	4,732,740	33.77 min	508 MB
Alternative approach 2	0.14895 mV/V	3,402,390	19.58 min	262 MB
Alternative approach 3	0.14432 mV/V	848,451	0.42 min	51 MB
Analytical approach	0.10838 mV/V	1	ad hoc (160 ms)	525 Bytes

[6] N. Hangst, S. Junk, and T. Wendt, “Verfahren zur Herstellung eines Roboterelements, insbesondere eines Greifers, mittels 3D-Druck,” US2020247044(A1), US US202016 776973 20200130, Aug 6, 2020.

[7] N. Hangst et al., ”Design of a 3D Printed Force Sensor in the Field of Robotics Utilizing an Embedded Constantan Wire as Sensing Element,” in ITG-Fachbericht, vol. 303, Sensoren und Messsysteme: Beiträge der 21. ITG/GMA-Fachtagung 10. - 11. Mai 2022 in Nürnberg, L. M. Reindl and J. Wöllenstein, Eds., Berlin, Offenbach: VDE VERLAG GmbH, 2022, pp. 74–80